

NUMERICAL SIMULATION OF TRANSIENT FLOWS IN A ROCKET PROPULSION NOZZLE

Suryakant P. Nagdewe, Hyeu Dong Kim

School of Mechanical Engineering,
Andong National University
388 Songchun-dong, Andong, Gyeongbuk, 760-749, Korea
surya@anuis.andong.ac.jp, kimhd@andong.ac.kr

Toshiaki Setoguchi

Department of Mechanical Engineering,
Saga University
Saga, Japan
setoguchi@me.saga-u.ac.jp

ABSTRACT

A numerical investigation of transient flows in an axisymmetric over-expanded thrust optimized contour nozzle is presented. These nozzles experience side-loads during start-up and shut-down operations, because of the flow separation at nozzle walls. Two types of flow separation such as FSS and RSS shock structure occur. A two-dimension numerical simulation has been carried out over an axisymmetric TOC nozzle to validate present results and investigate transient flow characteristics for start-up processes. Reynolds Averaged Navier-Stokes equations are numerically solved using a fully implicit finite volume scheme. Governing equations are solved by coupled implicit scheme. Reynolds Stress turbulence model is selected. Present computed pressure at the nozzle wall closely matched with experiment data. A hysteresis phenomenon has been observed between these two shock structures. The transition from FSS to RSS pattern during start-up process has shown maximum nozzle wall pressure. Nozzle wall pressure values have shown fluctuations during the FSS to RSS transition. The end-effect has been observed at high pressure ratio, when the recirculation bubble opens to the atmosphere.

INTRODUCTION

Large scale launch vehicle requires nozzle which can produce maximum specific impulse and thrust with reduced nozzle length. Until now, various supersonic nozzles such as Thrust Optimized Contour (TOC), Compressed Truncated Perfect (CTP) contours have been developed to meet such demands. TOC nozzles are currently used in Vulcain, Space Shuttle Main Engine (SSME) or J2S launcher engines. These rocket engines experience a long time of overexpanded operation with flow separation in transient phase at engine start-up or shut-down. In general, two separation patterns are observed, the free shock separation (FSS) and the restricted shock separation (RSS) (Nave et al., 1982). FSS structure can be observed in various types of nozzles such as conical contour nozzles and bell type nozzles including TP, TOC and CTP nozzles. In FSS, the flow separates fully from the nozzle wall due to an oblique shock that originates from the nozzle wall and is directed towards the nozzle centerline. The separated shear layer continues as a free jet (see figure 1). Since no reattachment occurs downstream of the separation location, this separation flow pattern is termed as free

shock separation. Downstream of the separation location, a back flow region exists where the ambient air is sucked into the nozzle due to the entrainment effect of the separated jet flow (Nagdewe et al., 2008). Nozzle flow fully separates from the wall at a certain ratio of wall to ambient pressure.

RSS is a peculiar type of the separation pattern which is observed only in TOC and CTP nozzles at a certain range of pressure ratio. In RSS, the flow separation is restricted over a short axial distance. The separated shear layer reattaches to the nozzle wall generating shocks and expansion waves. Due to the very short separated region, this flow regime is called restricted shock separation (see figure 2) (Nagdewe et al., 2008). This reattached flow results in wall pressures above ambient, which can initiate unsteady side-loads depending upon the asymmetry of the overall flow pattern, and oscillatory behavior of the associated shock system. The RSS separation pattern exists in nozzles which have the presence of internal shock because of the large divergent angle of nozzle wall. However, the presence of an internal shock in the nozzle does not require that RSS flow condition will appear ubiquitous. Both FSS and RSS can exist in such nozzles at different operating conditions. According to the previous work (Nave et al., 1982), it is known that the separation pattern evolves from FSS to RSS when the pressure ratio increases. Transitions between these two kinds of separation pattern present the hysteresis phenomenon. High peaks of side-loads are observed during transitions from FSS to RSS and vice versa. This hysteresis phenomenon appears typical during the start-up and the shut-down processes. Nguyen et al. (2003) highlighted an uncommon phenomenon at high pressure ratio for TOC nozzles. At high pressure ratios, separation structure repeatedly moves to downstream and upstream of the nozzle resulting in oscillation of nozzle wall pressure. This phenomenon is also called end-effect.

Chen et al. (1994) have first observed the reattached flow in their numerical simulations, and shown a trapped vortex immediately downstream of the central normal shock. Later, Nasuti et al. (1996) and Onofri et al. (1999), explained that an inviscid mechanism causes the generation of vortex which generates side-loads. Frey et al. (1999) have shown the existence of specific cap shock pattern which is a key driver for the transition from FSS to RSS and vice versa. On the other hand, Nguyen et al. (2003) have highlighted an uncommon phenomenon at high pressure ratio for TOC nozzles. The closed recirculation bubble at the

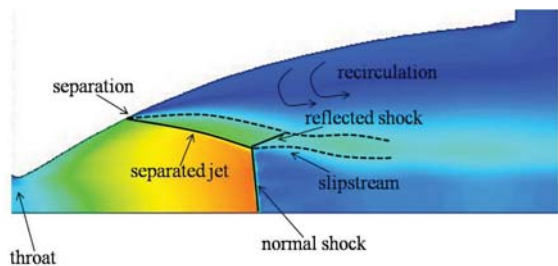


Figure 1: Free shock separation pattern (Nagdewe et al., 2008).

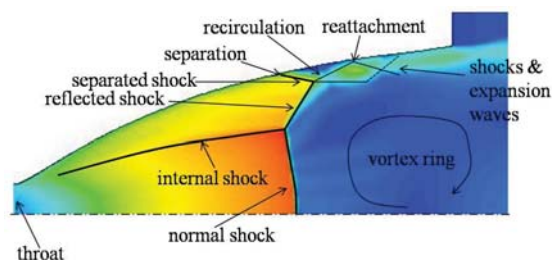


Figure 2: Restricted shock separation (Nagdewe et al., 2008).

nozzle wall opens to the ambience under the effect of the displacement of the separation structure downstream of the nozzle. Thereafter, separation structure moves upstream. This phenomenon called as end-effects, which induce a very high level of fluctuations. These experimental findings were numerically reconfirmed by Nebbache et al. (2006). The rocket engine transient side-load is a very complicated problem because it is a strongly unstable process. According to Hagemann et al. (2008), momentum balance across the cap-shock pattern, with the radial momentum towards the wall generated by the reflected internal shock causes the reattachment. While, Nasuti et al. (2008) have explained that the flow reattachment at the wall depends on the values and kind of upstream pressure gradient, irrespective of the existence of internal shock.

The literature review above has shown that rocket nozzles show the hysteresis effect, the transition of FSS to RSS and the end-effects at high pressure ratios. Numerical and experimental studies have been conducted to reveal the actual physics/mechanism behind the transition of FSS/RSS and side-loads. Many researchers have presented the occurrence of lateral side-loads but failed to explain the detailed mechanism. These unanswered questions are the motivation for the present work. In the present study, a computational fluid dynamic analysis of the transient flow during start-up has been carried out to investigate transient flow in rocket propulsion nozzle.

NUMERICAL PROCEDURE

Reynolds Averaged Navier-Stokes equations are numerically solved using a fully implicit finite volume scheme. Second order accuracy in space is achieved by using upwind method. The Reynolds Stress Model (RSM) is employed to close the governing equation systems, which are solved by a coupled implicit scheme. The RSM model is considered in present work because it is a most elaborate turbulence model, which considers anisotropic eddy viscosity hypothesis. It is appropriate for unsteady calculations while other turbulence models are based on time-average treatment. It

reflects the effects of streamline curvature, swirl, rotation, and rapid changes in strain rate in a more rigorous manner than one-equation and two-equation models.

Computational domain consists of a typical TOC nozzle as shown in figure 3. TOC nozzle consists of r_e and r_i as the nozzle exit and inlet radius respectively. Throat radius r_t considered is 0.01362 m and length of nozzle is approximately $15r_t$. Computational grid has 560 points in axial direction (460 points inside the nozzle) and 121 points in radial direction. Total numbers of grid cells are 67,760. The total length of computational domain is $300r_t$ in axial direction and $40r_t$ in radial direction. Boundary conditions at inlet are considered as total pressure (P_o) and total temperature (T_o). At outlet boundary, static pressure (P_a) was given as a back pressure (figure 3). The mesh is clustered close to nozzle wall in order to have a y^+ value less than 1.

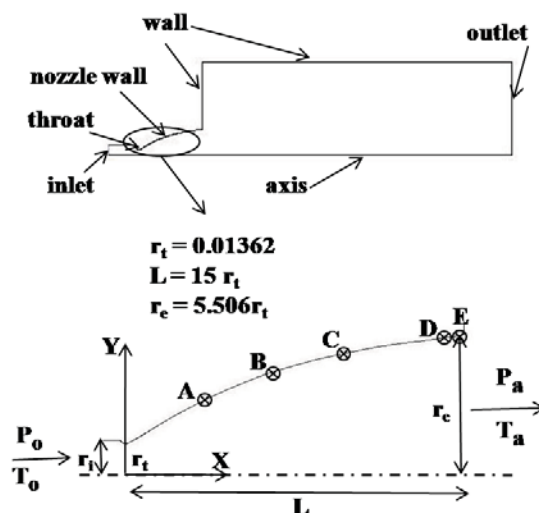


Figure 3: Computational domain with boundary conditions and nozzle geometry.

The steady state pressure ratio (P_o/P_a) of 10.2 is considered as the beginning of start-up process. Total pressure and total temperature values at inlet are $P_o = 10.2 \times 10^5 Pa$ and $T_o = 270K$. Computational domain is initialized by $P_a = 10^5 Pa$, $T_a = 288K$ with zero velocities. Next steady state computation uses the previous computed flow field as an initial condition. An unsteady calculation has been carried out by changing the flow boundary conditions. Pressure ratio is increased in the computational procedure of the start-up transient process. Pressure ratio is increased by 1 for 1 ms to have a linear increment, followed by a stabilization period of 9 ms. This is with regards to the experiment carried out for 10 ms for a particular pressure ratio. The computation is repeated till the desire pressure ratio is achieved.

RESULTS AND DISCUSSION

A validation study has been carried out for a pressure ratio of 10.2, 15.4 and 20. figure 4 shows the comparison of present wall pressure (P_w) distributions along the nozzle wall with experiment (Nguyen, 2003) and CFD by Nebbache et al. (2006). Present computational results show good match with experiment data and CFD by Nebbache et al. (2006).

The FSS structure was observed for the pressure ratio 10.2, 15.4, 18 and 20. In FSS, boundary layer separates,

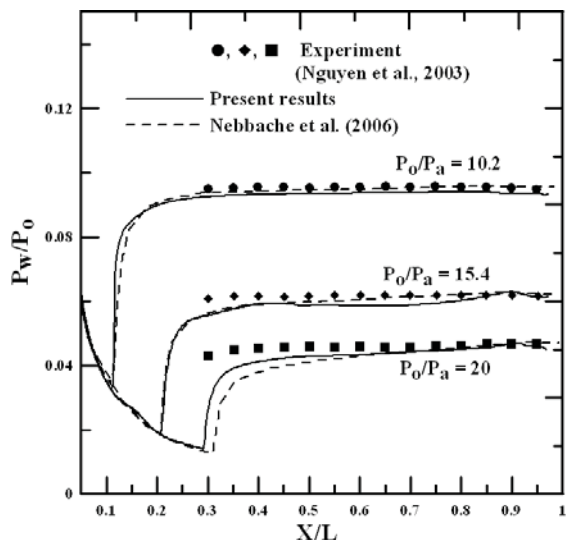


Figure 4: Comparison of present wall pressure distributions along the nozzle wall.

and never reattaches to nozzle wall (figure 1). The transition from FSS to RSS is seen by increasing pressure ratio from 20.0 to 23.9. Cap-like shock structure, which generates during increase in pressure ratio, forces the separated boundary layer to reattach on the nozzle wall (see figure 2). The RSS pattern was obtained for pressure ratio 23.9 or by decreasing the pressure ratio from 23.9 to 18.0 and further to 13.0. The FSS pattern is observed again when the pressure ratio is decreased from 13.0 to 12.0. Thus, the hysteresis cycle between the FSS and RSS is obtained (figure 5). Present numerical calculations have shown hysteresis cycle in the range of pressure of 12 to 23.9 against experiment range of 12 to 24 (Nguyen, 2006). Mach number plot (figure 6) at pressure ratio 18, show FSS and RSS during start-up and shutdown processes of rocket nozzle.

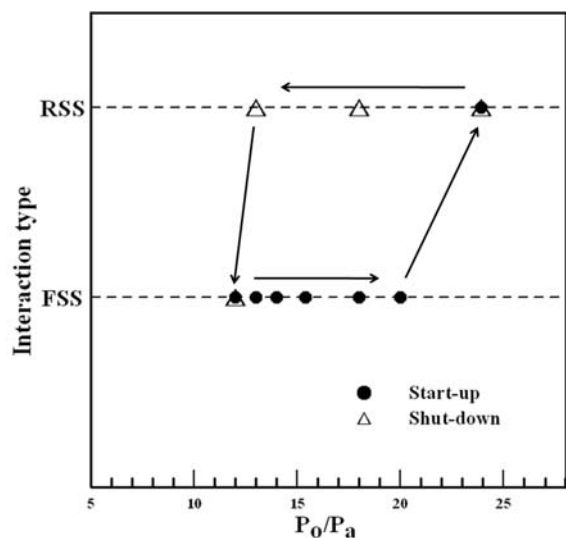


Figure 5: Hysteresis cycle observed in present CFD.

The transition of FSS to RSS occurs during start-up process, when pressure ratio is increased from 20.0 to 22.0. Pressure ratio is increased linearly in two steps. In first step, pressure ratio is linearly increased from 20.0 to 21.0 in 1 ms followed by a stabilization period of 9 ms. Second step comprises linear increment of pressure ratio from 21.0 to 22.0 in

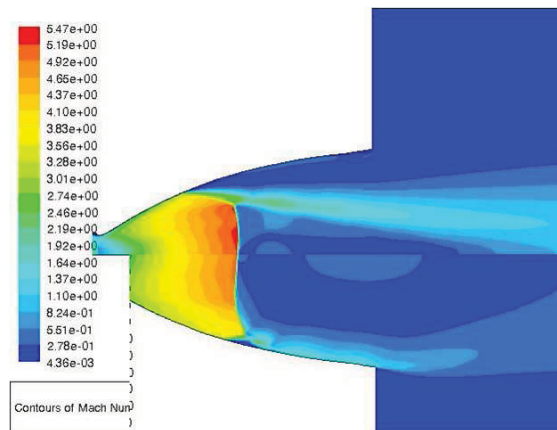


Figure 6: Mach number plot at NPR 18 for start-up and shut-down processes (top FSS and bottom RSS).

1 ms. At $t = 0.001$ s, FSS shock structure is observed, which is at pressure ratio 20, and shows absence of wall pressure (P_w) fluctuations. As the pressure ratio linearly increased, cap-shock pattern slowly appears (see figure 2). Initially, we can observe that the pressure remains very close to the ambient pressure, $P_a = 10^5 Pa$, downstream of the shock structure (figure 7). The shock structure moves downstream of the nozzle, as the pressure ratio increase. Separation point move downstream because of the static pressure is less than the ambient in the recirculation bubble between separation and reattachment point. The wall pressure at the nozzle exit increases to reach the external value P_a . Oscillations of wall pressure around P_a appear at $t = 0.0067$ s and develop strongly in the reattaching region starting from $t = 0.0075$ s, as shown in figures 7 and 8.

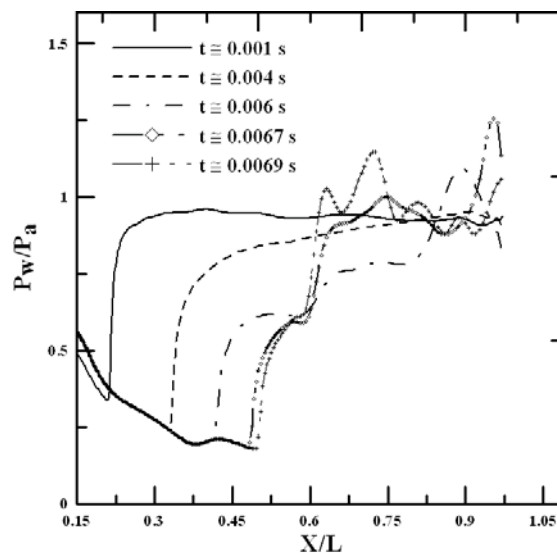


Figure 7: Time dependent wall pressure distributions for start-up process ($t = 0.001$ to $t = 0.0069$ s).

These wall pressure fluctuations occur due to expansion and compression waves being reflected between the wall and central recirculating vortex. We can observe the maximum wall pressure during this transition is close to $2.0 \times 10^5 Pa$. Wall pressure profiles at location A, B and C are shown in figure 9, where $P_w(t)$ represents time history of wall pressure. $P_w(t), avg$ is the average values over the time t . Location A is at the upstream of separation, while B and

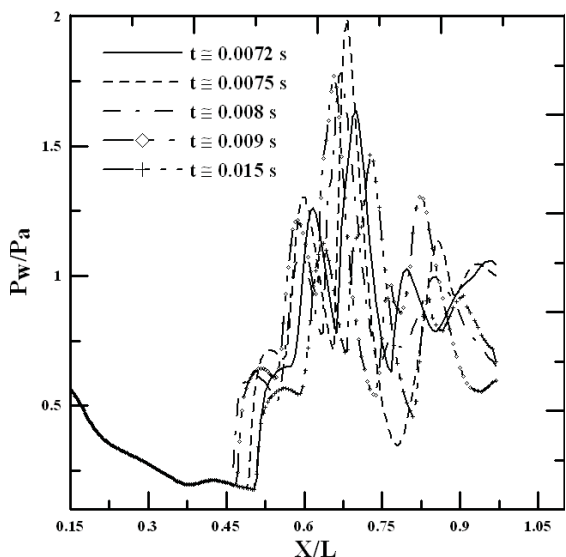


Figure 8: Time dependent wall pressure distributions for start-up process ($t = 0.0072$ to $t = 0.015$ s).

C are at the downstream. Fluctuations in wall pressure are observed during transition of FSS to RSS at location A. Location B and C, being at the downstream of separation, have not shown fluctuations. This high value of pressure means that, a small asymmetry of the flow can give important side-loads. Thus, the origin of side-loads in thrust optimized nozzle is due to the transition of FSS to RSS.

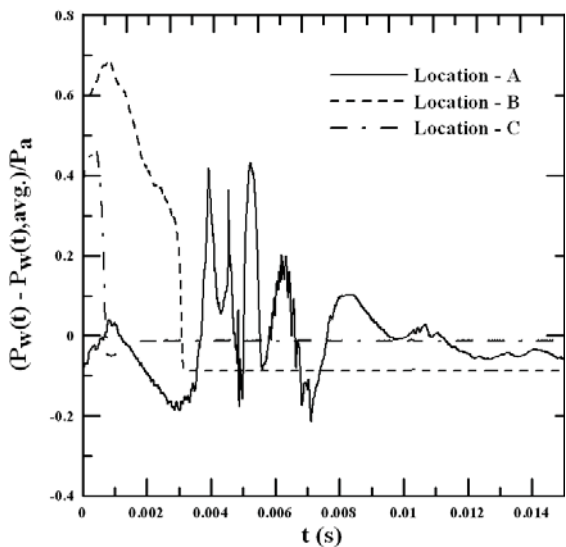


Figure 9: Time dependent wall pressure distributions for start-up process at location A, B and C.

Increase in pressure ratio, moves recirculation bubble downstream and the reattachment point reaches the nozzle exit. At certain pressure ratio, longitudinal movement of separation structure occur, which is reported by Frey et al. (1999) and observed in experiment by Nguyen et al. (2003). An unsteady numerical simulation is carried out for a pressure ratio 48.2. Numerical simulation is conducted for 0.05 s. The recirculation bubble opens to the atmosphere where ambient pressure P_a is close to 10^5 Pa, and the recirculation zone pressure decreases to values lower than the ambient pressure. At this time, the local pressure gradient is reversed and the separation point moves upstream. Thus, the recir-

culation zone closes and the bubble is generated once again. This opening-closing process of the recirculation bubble is observed repeatedly many times at the fixed pressure ratio of 48.2. Figures 10 and 11 show the shock structure patterns at different times. At $t = 11.6$ ms, the shock structure is located at its nearest position from the nozzle throat. As time passes, this structure moves downstream. The reattachment point of recirculating bubble comes near the nozzle exit, and the wall pressure initially larger than ambient pressure decreases gradually. The opening of the recirculation bubble is clearly visible at $t = 12.8$ ms, is accompanied by a decrease of wall pressure due to the mixing with the reverse flow from the ambience. This also provokes a strong defect of different mixing layer away from the nozzle axis. The closing of the recirculation bubble is followed by the upstream movement of the separation shock, which is the beginning of a new cycle.

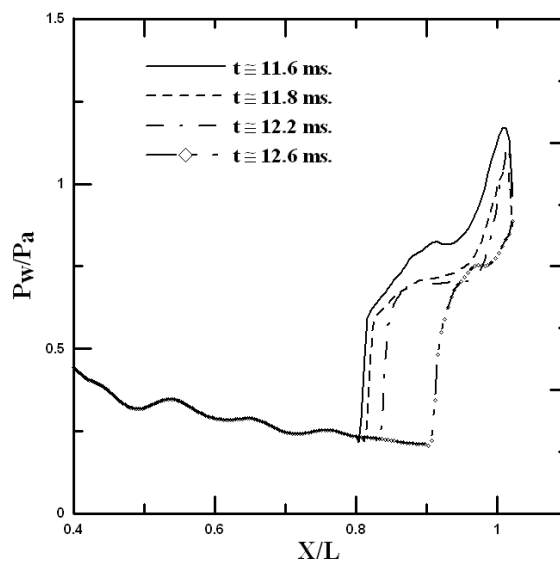


Figure 10: Time dependent wall pressure distributions for start-up process ($t = 11.6$ to $t = 12.6$ ms).

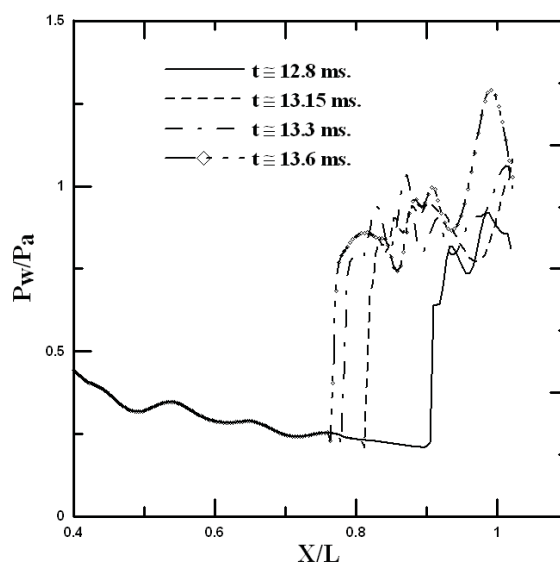


Figure 11: Time dependent wall pressure distributions for start-up process ($t = 12.8$ to $t = 13.6$ ms).

CONCLUSION

A numerical investigation of axisymmetric thrust-optimized contour nozzle flow separation has been performed with RSM turbulence model. Present computational results are in good agreement with experiment data and other numerical ones. The numerical simulations have shown hysteresis phenomenon between the free shock separation (FSS) and the restricted shock separation (RSS). The transition from FSS to RSS pattern is numerically reproduced during start-up process. Peaks in wall pressure are observed during the transition. At high pressure ratio, the recirculation bubble opens to the atmosphere and then closes, has been observed.

REFERENCES

- Chen, C. L., and Chakravarthy, S. R., and Hung, C. M., 1994, "Numerical investigation of separated nozzle flows", *AIAA Journal*, Vol. 32, No. 9.
- Frey, M., and Hagemann, G., 1999, "Flow separation and side-loads in rocket nozzles", *AIAA 99-2815*.
- Hagemann, G., and Frey, M., 2008, "Shock pattern in the plume of rocket nozzle: needs for design consideration", *Shock Waves*, Vol. 17, pp. 387-395.
- Nave, L. H., and Coffey, G. A., 1973, "Sea levels side loads in high-area-ratio rocket engines", *AIAA Paper 73-1284*.
- Nagdewe, S. P., and Kim, H. D., 2008, "A computational study on the unsteady lateral loads in a rocket nozzle", *Proceedings, Korean Society for Propulsion Engineers*, KAIST, Daejeon.
- Nguyen, A. T., and Deniau, H., and Girard, S., and Roquefort, T. A., 2003, "Unsteadiness of flow separation and end-effects regime in a thrust-optimized contour rocket nozzle", *Flow, Turbulence and Combustion*, Vol. 71, pp. 161-181.
- Nasuti, F., and Onofri, M. 1996, "Viscous and inviscid vortex generation during nozzle flow transients", *AIAA Paper 96-0076*.
- Nasuti, F., and Onofri, M., 2008, "Shock structure in separated nozzle flows", *Shock Waves*, DOI 10.1007/s00193-008-0173-7, published online.
- Nebbache, A., and Pilinski, C., 2006, "Pulsatory phenomenon in thrust-optimized contour nozzle", *Aerospace Science and Technology*, Vol. 10, pp. 295-308.
- Onofri, M., and Nasuti, F., 1999, "The physical origins of side-loads in rocket nozzles", *AIAA Paper 99-2587*.